

AA236B Report: Deployable Sunshade Mechanism Design for Next Generation Telescope

Spacecraft Design Laboratory, Stanford

Yasmina Elmore, Melanny Garcia, Samuel Montagut Agudelo

March 21, 2025

1 Introduction

1.1 General concept

The next generation of space telescopes demands a precise optical environment, free from stray light interference and maintained within stringent thermal bounds. To address these needs, our team has been tasked with designing a deployable sunshade that protects the telescope's instruments from unwanted illumination while simultaneously regulating its temperature.

At full deployment, the sunshade must span an area of $20\text{ m} \times 20\text{ m}$ in three layers, each made of $50\text{ }\mu\text{m}$ -thick Kapton coated with a 100 nm aluminum layer and spaced 10 cm apart. This large-scale membrane structure must survive a wide thermal range, resist micrometeoroid damage, and still fit within a $0.5\text{ m} \times 0.5\text{ m} \times 0.3\text{ m}$ stowed volume. Additionally, it is constrained to a total mass of less than 200 kg and must achieve a first-mode frequency above 0.1 Hz to ensure adequate stiffness once deployed. Balancing these stringent performance, mechanical, and environmental requirements represents a significant engineering challenge, forming the foundation of the work detailed in this report.

This report discusses the concept, prototyping, building, and testing realized on a designed deployable structure during this project. Chapter 1 specifies the different notions and introduces the requirements necessary in order to define the concept. Chapter 2 turns around the choice of the prototype and how to meet the requirements. Chapter 3 delves deeper into the building and fabrication of the mechanism. Chapter 4 covers the testing of the built prototype. Finally, Chapter 5 introduces a discussion on the results obtained and offers a vision on how the design could be improved.

1.2 Requirements

This section introduces the requirements that will define the design of the system. We differentiate the key requirements and the driving requirements. The requirements are summarized in Table 1 and we can identify requirements **R1**, **R2**, **R3**, **R4**, **R10** and **R11** as key requirements of the system.

Number	Description	Requirement
R1	Sunshade deployed area	$20\text{ m} \times 20\text{ m}$
R2	Number of sunshade layers	3 layers
R3	Membrane material	$50\text{ }\mu\text{m}$ Kapton with 100 nm Aluminum
R4	Separation between layers	10 cm
R5	Separation when operating	Required
R6	Mass	$< 200\text{ kg}$
R7	Stowed volume	$< 0.5\text{ m} \times 0.5\text{ m} \times 0.3\text{ m}$
R8	First mode frequency	$> 0.1\text{ Hz}$
R9	Spacecraft bus interface	$0.5\text{ m} \times 0.5\text{ m}$
R10	Thermal environment	$-178^\circ\text{C} < T < 150^\circ\text{C}$
R11	Membrane tears spreading	$< 2\text{ m} \times 2\text{ m}$
R12	Venting of sunshade layers	Required

Table 1: Project Requirements Table

The requirements will be studied in order to define an order of magnitude for some components of the spacecraft. However, in our case, we are limited by the size of the spacecraft we are going to build. Therefore, we would need to reconsider the scaling of the satellite. In the next section, we will discuss how we can define and quantify the different components, while also addressing the choice of rescaling for our specific application.

2 Design

This chapter describes the design and rationale behind every component of the deployable sunshade-boom sub-system for satellite design, and focuses on how each element meets the requirements defined in

Section 1.2.

2.1 Concept Description

The satellite design is based on two primary configurations: the stowed configuration and the deployed configuration. In the stowed state, the sunshade consisting of a three-layer membrane is folded using a flasher pattern in order to optimize the packing efficiency. The outer edges of the membrane are attached to four deployable booms, built and designed from tape springs. Initially, these booms are coiled and then deploy outward in a controlled manner, driven by a brushless DC motor. Once fully deployed, the layers are separated using telescoping masts located at each end of the booms and carefully attached to the layers. Figure 3 presents an overview of the concept for a deployable sunshield mechanism, where the sunshield is composed of three distinct layers. However, the figure does not represent the correct scale.

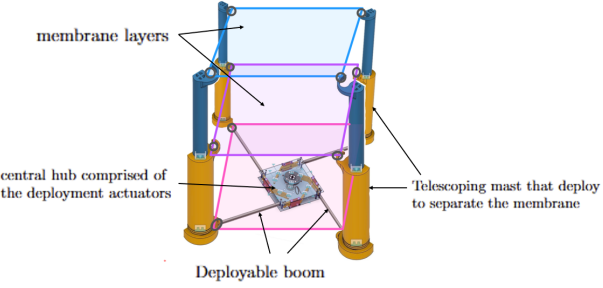


Figure 1: Concept Overview of the Deployable Sunshield

Mechanism Description. In order to meet the demanding requirements of stowage efficiency, mass minimization, and reliability, a Carbon Fiber shearless boom mechanism is used for deployment. Similar to what is shown in [Fer17], booms can be designed to be bistable, meaning they can remain tightly coiled in a stable state and then snap into a second stable state upon deployment. These booms are typically made from thin composite laminates that exploit the material's anisotropy to achieve the desired bistability.

During storage, shearless composite booms are coiled in an Archimedean spiral, requiring minimal external constraint. Once the central motor initiates deployment, the transition zone between the coiled and deployed portions of the boom travels outwards; the stored strain energy in the laminate helps drive the deployment. This approach greatly simplifies the mechanical design of the sunshade because it mini-

mizes complex latch or hold-down mechanisms. Additionally, carbon composite booms are known for their high specific stiffness and strength, which helps meet both the mass and first-mode frequency requirements.

2.2 Design Rationale

To justify the design rationale, it is essential to understand the three pillars of engineering: theory, simulations, and experiments. The pillars are interconnected through verification, validation, and model calibration.

- Verification connects theory and simulations, ensuring that the computational models correctly implement the theoretical equations.
- Validation connects theory and experiments, confirming that the theoretical predictions align with real-world experimental results.
- Model Calibration involves adjusting the parameters in a simulation model so that its predictions match experimental data.

2.3 Flasher Pattern

Let's begin by justifying the design of the flasher pattern. According to requirements **R3** and **R7**, we must design a membrane composed of a $50 \mu\text{m}$ Kapton sheet with a 100 nm aluminum coating, which must fit within a stowed volume of $0.5 \text{ m} \times 0.5 \text{ m} \times 0.3 \text{ m}$. To meet these specifications, the membrane must be folded using specific patterns to optimize its stowing efficiency. For this purpose, we employ the origami flasher pattern, which has been proven successful in deployable spacecraft structures due to its well-established stowage efficiency. Figure 2 illustrates the sequential unfolding of the flasher pattern membrane.

Several parameters must be considered to characterize the pattern properly (*e.g.*, order m , height order h , ring order r , separation between vertices dr , scaling factor s_f). All of these parameters can be determined using documented code such as that developed by Shannon A. Zirbel *et al.* in their work on origami-based deployable structures. To generate a flasher pattern that meets these constraints, we utilized Mathematica code developed by Robert Lang, which allowed us to specify key geometric parameters that influence the stowage efficiency and deployment characteristics of the membrane as seen in [Lan97] and [ZLT⁺13]. The selection of these parameters was driven by the need to achieve a compact folded configuration while ensuring a smooth and reliable unfolding process. Given that the membrane

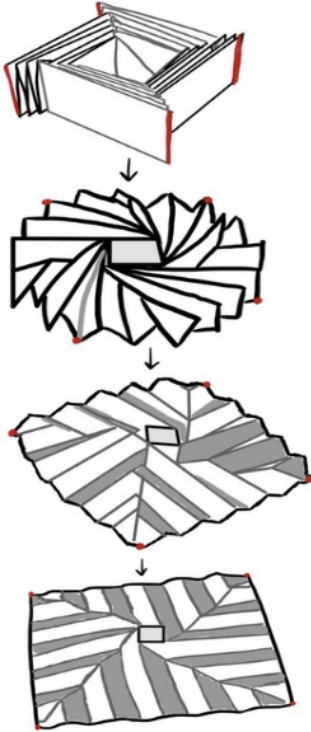


Figure 2: Unfolding Sequence of a Flasher Pattern

must expand from its tightly stowed form to a fully deployed $20\text{ m} \times 20\text{ m}$ configuration, it was critical to balance compactness with the need to avoid excessive material strain or complex deployment dynamics. One of the primary parameters influencing the folding geometry is the flasher order, m , which determines the number of radial fold sections. Increasing the order results in a more compact stowed form but introduces additional creases, which can impact deployment by increasing the complexity of unfolding forces. A higher flasher order allows for greater radial symmetry, which is beneficial for even stress distribution during deployment. However, increasing this value too much can lead to a higher density of folds that may introduce excessive material stress in the Kapton sheet. The selected order was chosen to balance these factors, ensuring that the pattern achieved the required stowage volume while maintaining deployability. The height order, h , is another critical parameter that affects how the folds are stacked within the stowed volume. This parameter influences the thickness of the folded stack and plays a direct role in ensuring that the membrane remains within the 0.3 m stowed height constraint. By adjusting the height order, we controlled the vertical stacking density, preventing excessive compression forces that could damage the thin-film structure. This parameter

was selected to maintain an optimal folding ratio, ensuring that the compressed layers remained uniform and did not introduce localized bulging that could disrupt deployment. Additionally, the ring order, r , was carefully chosen to determine the number of concentric folding rings. Increasing the number of rings results in a more uniform stowage distribution, reducing stress concentrations at the center of the pattern and allowing for a smoother unfolding process. However, a higher ring order also requires more precise manufacturing tolerances to ensure proper alignment during folding. The chosen value of r provided an optimal compromise between stowage compactness and deployment predictability, ensuring that the membrane could be fabricated with practical precision while maintaining efficient packing. The separation between vertices, dr , played a significant role in controlling the amount of strain experienced by the Kapton film during folding. This parameter dictates how far apart adjacent folds are positioned, influencing the local curvature of the material. A smaller vertex separation allows for a more compact fold but can introduce higher bending stresses that may compromise material integrity over repeated deployment cycles. Conversely, a larger vertex separation results in a looser fold that reduces material stress but increases the overall stowage volume. The selected separation was carefully tuned to prevent excessive stress concentrations while maximizing the compression ratio of the stowed membrane. Each of these parameters

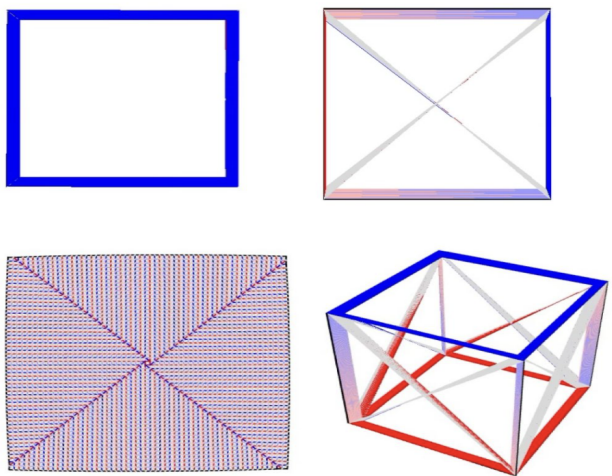


Figure 3: Simulation of Chosen Parameters for the Flasher Pattern

was systematically adjusted to create a folding pattern that met the mission's stowage and deployment requirements as seen in [LMH16]. For these parameters, we selected parameters of $[r, h, m, dr]$ to be [16,

5, 4, 0.05]. The final pattern was selected based on its ability to balance high stowage efficiency, minimal material strain, and reliable unfolding behavior, ensuring that the membrane would deploy consistently while maintaining its structural integrity. The use of computational origami techniques allowed for the precise control of these geometric properties, providing a rigorously optimized folding scheme that aligns with the constraints imposed by spacecraft packaging and deployment dynamics.

2.4 Deployable Booms

The deployable booms in the sunshade system are critical to extending and supporting the large three-layer membrane while maintaining structural integrity. They must be lightweight, occupy minimal volume in the stowed configuration, and reliably deploy to their full length without risk of jamming or failure.

In the stowed configuration, the booms are coiled on a central spindle. Upon actuation, a motor unwinds the booms, extending them radially. This motion tensions the membrane and guides the sunshade to its final geometry.

Key Advantages:

- **Simplicity:** Bistable Carbon Fiber Reinforced Polymer (CFRP) booms do not typically require complex hold-down or spring-driven release mechanisms; they remain stable in both the coiled and deployed states.
- **Ease of Fabrication:** While CFRP manufacturing does demand careful control of the layup process, modern composite fabrication techniques are well-established, making the process repeatable and robust.
- **Flight-Proven Heritage:** CFRP tape-spring booms have already been used in multiple space-flight applications for deployable antennas, solar sails, and drag sails, providing a confidence level that benefits new missions.
- **High Stiffness-to-Mass Ratio:** The inherent stiffness of carbon fiber helps achieve the first-mode frequency requirement without adding significant weight.

There are different types of booms. We distinguish among them the Collapsible Tubular Mast (CTM) boom, the TRAC boom, and finally the SHEAth-based Rollable lenular-shaped with Low friction (SHEARLESS) boom [Fer17]. An illustration of the different booms is offered in Figure 4.



Figure 4: Illustration of manufactured CTM, TRAC and SHEARLESS boom[Fer17]

The prototype will consider the advantages of the SHEARLESS boom. The SHEARLESS boom comprises an opposite-sense coiling composite tape spring and an equal-sense coiling composite tape spring. The two tape springs are wrapped in a seamless sleeve, which helps maintain the integrity of the entire structure. A representation of a coiled SHEARLESS boom is given in Figure 5.



Figure 5: Illustration of the coiling of a SHEARLESS Boom [Fer17]

2.5 Central Mechanism

The central mechanism encompasses the hub, motor, and adjoining structure that collectively manage the deployment of the shearless-composite booms and the sunshade membranes. Its design was chosen specifically for:

- **Simplicity in Operation:** By leveraging the

bistable nature of the booms, the central hub only needs to rotate at a controlled rate to “push” or guide the booms outward. This greatly reduces the number of moving parts compared to mechanisms that must also clamp or hold tension in the stowed state.

- **Ease of Fabrication:** The hub itself can be made from standard aerospace-grade aluminum or similarly machinable metals. The key requirement is to provide a smooth guiding channel and appropriate rollers (or low-friction interfaces) for the coils.
- **Flight-Proven Heritage:** Mechanisms closely resembling this approach have been used in deorbit drag-sail systems and solar sail deployments [FSP⁺13]. Reusing proven design principles lowers risk and ensures predictable performance.



Figure 6: Mechanism designed by NASA [FSP⁺13] that inspired our central hub

2.5.1 How It Works

1. **Coiled State:** Each shearless boom is wrapped in a stable coiled configuration around the hub. Only minimal restraints (or none at all, if the booms are purely bistable) are needed to keep the booms from partially deploying during launch.
2. **Initiation:** A brushless DC motor, located at the center of the hub, begins rotating. This rotation unspools each boom in turn, effectively “pushing” the boundary between the coiled and uncoiled sections outward.
3. **Transition Zone Propagation:** As the hub continues rotating, the transition zone between coiled and deployed states travels along each boom. The stored strain energy assists in stabilizing the new shape, removing the need for forceful extension or heavy springs.

4. **Full Deployment:** Once the booms reach their full length, the motor stops. At this point, the booms are in their second stable state, providing a stiff, lightweight support structure for the sun-shade layers. Any minor adjustments or tensioning can be managed by the motor or small latching elements if necessary.

In summary, the central mechanism’s design focuses on reliability and minimal complexity. The choice of a CFRP bistable deployment system is driven by the need to meet strict constraints on stowed volume, mass, and dynamic performance, as well as the desire to rely on a flight-proven architecture [Fer17]. By combining these advantages, the mechanism effectively balances low mass, compactness, and structural robustness.

3 Prototyping

To validate the design and deployment mechanics of the sunshade system, a scaled-down prototype was developed. Although it does not use the same space-grade materials as the intended flight model, it captures the essential structural and functional principles of the full-scale design. This prototype employs cost-effective alternatives—such as PLA for structural components, Stanley FATMAX tape measures for bistable booms, and Mylar sheets for the membrane—allowing for rapid iteration and refinement while retaining key deployment characteristics.

A series of tests on the central hub, booms, and membrane deployment mechanisms aimed to uncover potential failure modes, including coil “blossoming,” friction-induced irregularities, and misalignment of moving parts. The following sections describe the prototype’s specifications, the materials used, and the fabrication techniques that enabled the successful demonstration of the deployable sunshade concept.

3.1 Central Mechanism

3.1.1 Central Hub

The central hub underwent multiple design iterations in response to both mechanical and manufacturing challenges. In the earliest version, the hub was designed to fit a 4 mm shaft on a DC brushed motor via a press fit. A needle roller bearing was also press-fit into the bottom portion of the hub to facilitate smooth and centered rotation around the motor holder. Figure 7 shows one of the initial CAD models featuring angled inserts to guide the coiling of the booms and ensure proper alignment.

In parallel, a steel hub concept was explored, as shown in Figure 8, in which the booms would be

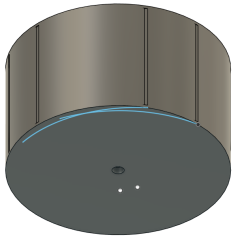


Figure 7: CAD of an Early Hub Design with Angled Inserts.

welded directly to the steel hub. This approach was intended to eliminate the risk of detachment at the hub-boom interface and to mitigate any stripping at the motor interface. Ultimately, this steel hub concept was abandoned due to limited CNC milling capabilities.



Figure 8: CAD of a Steel Hub Concept with Welded Boom Mounts.

Subsequently, the motor was changed to a 6 mm D-shaft configuration, which necessitated a shorter overall hub. The design had to be revised three times to accommodate the motor's new shaft geometry and length. Despite these changes, several plastic hub prototypes stripped under motor torque. A resin-based hub (Figure 9) also failed, as resin filled critical slots and did not adequately secure the motor shaft.



Figure 9: 3D-printed Resin Hub Prototype. The Filled Slits Made it Ineffective for this Application.

Ultimately, a PLA-printed hub used in conjunction with a metal shaft coupler proved successful. The bearing press-fit was preserved to maintain smooth rotation, and the hub was designed with six mounting holes to mate securely with the shaft coupler. The final assembly of the motor holder, bearing, and hub is shown in Figure 10.

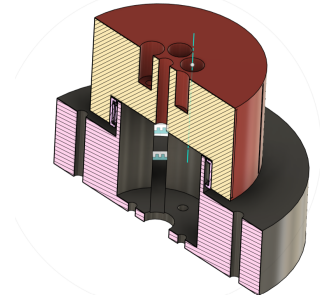


Figure 10: Final Assembly of the Motor Holder, Bearing, and PLA-Printed Hub with Shaft Coupler.

3.1.2 Motor

Initially, a 12 V brushed DC motor with a 4 mm nominal shaft was selected because it fit within the allowable volume and was presumed to provide the highest torque density for its size. During testing, however, the motor's rotational speed—even with a speed controller—proved difficult to manage, and the torque was inadequate for consistent deployment.

As a result, a geared motor with a 6 mm D-shaft was procured on short notice (Figures 11, 12, and 56). This change required redesigning the motor holder and the hub. Despite the additional effort, the geared motor ultimately supplied the desired torque and a more suitable rotational speed for deployment.

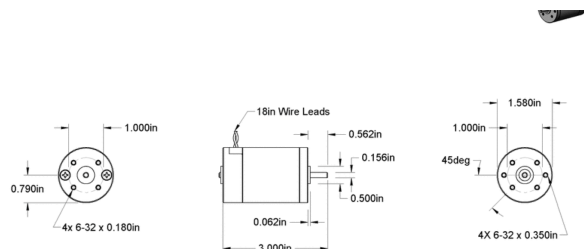


Figure 11: Dimensional Drawing of the Original 4 mm Shaft Motor.

3.1.3 Structure

The central mechanism's structural frame occupies a 30 cm × 30 cm footprint with an overall height of



Figure 12: Photograph of the Original 4 mm Shaft Motor.



Figure 13: Geared Motor with a 6 mm D-shaft, Providing Improved Speed and Torque.

approximately 5 cm. This low-profile design was chosen early on to maximize the available volume for the membrane layers. The structure consists of two acrylic plates joined by 4mm screws and separated by 41 mm spacers. Wave washers and low-profile nuts were used to minimize thickness and ensure that the assembly remains secure under load.

In addition to connecting the two plates, the spacers serve several key functions:

- **Boom Guides:** Four pairs of spacers create channels through which the booms deploy radially at right angles, ensuring controlled and consistent deployment directions.
- **Spring Arms Pivot Points:** Four of the screws also act as pivot axes for torsion spring arms that help prevent coil blossoming (Section 3.1.4).
- **Spring Arm Standoff Features:** A small 3D-printed component is used as a standoff, providing a surface for one leg of each torsion spring to push against.

Finally, the center of each acrylic plate includes cutouts to accommodate the motor shaft, motor holder, and the hub. These cutouts also provide attachment points for the motor holder, ensuring that all central mechanism components are securely integrated. Figures 14 and 15 illustrate both the CAD model and the assembled structure.

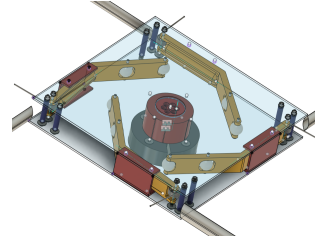


Figure 14: CAD of the Central Structure.

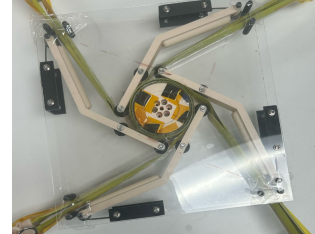


Figure 15: Central Structure After Assembly.

3.1.4 Blossoming Springs

To prevent the coiled booms from blossoming outward during deployment, each boom passes beneath a spring-loaded arm. These arms use small rollers at the contact points to reduce friction while maintaining inward pressure on the coils. Initially, a stiffer torsion spring designed for the 4mm pivot shaft was attempted; however, it proved too weak for the final design.

To resolve this, a PLA spacer was added to increase the pivot shaft diameter, allowing use of a larger 12 in · lb torsion spring that provided the necessary preload. The spring arm itself was also iterated to better accommodate the spring's leg, while a small stopper feature anchors the opposing leg. Figure 16 shows the final CAD design of the torsion spring arm system.



Figure 16: CAD of the Final Torsion Spring Arm System.

3.2 Booms

Unlike the full-scale flight system, which would require four booms extending a 20 m × 20 m mem-

brane, our prototype was built to a $1.2\text{ m} \times 1.2\text{ m}$ scale due to lab constraints.

3.2.1 Telescoping Rods

The telescoping rods were implemented in the prototype to mimic the vertical separation of membrane layers in the full-scale flight system. These rods acted as temporary deployment guides, ensuring that the sunshade structure unfolded correctly and that the three layers remained evenly spaced throughout the deployment process. The rods were designed to be spring-loaded, providing a controlled extension mechanism while minimizing resistance during deployment. Each rod was constructed from lightweight sliding tubes, which were capped with 3D-printed PLA end fittings. The use of PLA caps allowed for easy customization of attachment interfaces, ensuring a secure connection between the rods and the membrane without introducing excessive stress at the attachment points. A 10 cm long internal spring inside each rod provided the necessary extension force, allowing the rods to extend automatically once the deployment sequence was initiated. To integrate the telescoping rods into the overall structure, a boom-rod interface system was developed. This interface consisted of custom-designed clips that attached to both the membrane and the base structure, ensuring that the rods remained in the correct position during stowage and deployment. These clips were designed to minimize stress concentrations, preventing localized deformation or misalignment of the rods. Additionally, the rods featured a low-friction sliding mechanism, allowing for smooth extension without unnecessary resistance. Fabrication of the telescoping rods involved precision cutting and assembly of the sliding tubes, ensuring consistent fit and movement across all four rods. The springs were sized based on the required deployment force, and each rod was manually assembled, with the springs inserted into the sliding tube system before being secured with the PLA caps. The final assembly ensured that the telescoping rods provided uniform separation between the sunshade layers while maintaining a compact, stowable form factor.

3.2.2 Tape Springs

For prototyping, the tape springs needed to retain some of the key characteristics of the flight-design booms, such as being lightweight, bistable, coilable, and durable. The choice of material for prototyping was based on its availability and the ability to use it without additional manufacturing. The material selected for the booms was steel coated with Mylar, commonly found in measuring tapes such as STAN-

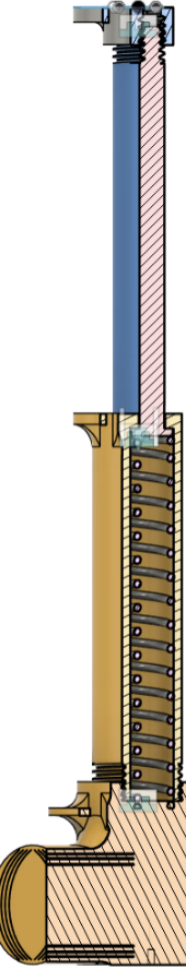


Figure 17: CAD of Telescoping Rod Components

LEY FATMAX tapes, as shown in Figure 24.



Figure 18: STANLEY FATMAX used for Deployable Booms



Figure 19: STANLEY FATMAX Coiling

The properties and geometry of the STANLEY tape spring are defined in Table 2

Each boom was composed of an "inner tape spring" and an "outer tape spring" that had different lengths. The inner tape springs were cut to 33.5 cm long, and the outer tape springs were cut to 35 cm long to meet the dimensions of the membrane. The reason for this difference in length is the way the tape springs are attached to the central hub; there is a difference of a couple of centimeters between where the inner tape spring is attached to the hub and where the outer tape spring is attached to the hub.

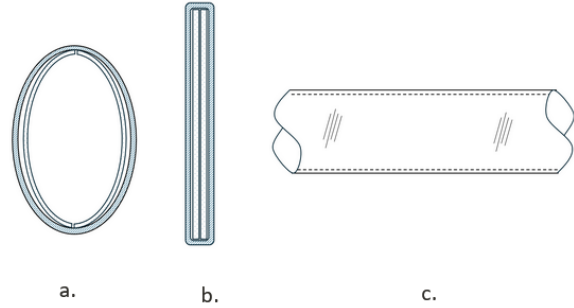
3.2.3 Shearless Sleeve

The shearless booms are made of two tape springs, an inner and an outer tape spring, wrapped together in a shearless sleeve. The sleeve plays an important part in maintaining the overall shape of the boom, whether it is coiled or deployed, while ensuring that no internal deformation is linked to transverse force. Figure 20 illustrates how the sleeve fits booms.

To build a sleeve, it is essential to prioritize materials such as Kapton, Teflon, and Fluorinated Ethylene Propylene (FEP), which are affordable heat-resistant polymers with a seamless structure. Given its affordability, compatibility with Kapton tape, and high

Property	Description
Material	High-carbon steel
Coat	with Mylar coating
Young's Modulus E	210 GPa
Yield strength σ_Y	1500 MPa
Poisson's ratio ν	0.28
Length L	33.5 cm or 35 cm
Thickness t	0.15 mm
Width w	32 mm
Radius of curvature R	3.122 cm
Radius of coiling r	2.271 cm

Table 2: Material Properties and Geometry of STANLEY FATMAX tape Spring. The data were either collected from the official website [Sta25] or measured in class.



a. cross sectional view of the booms inside the sleeve
b. cross sectional view of the flattened booms inside the sleeve
c. Side view of the sleeve

Figure 20: Sketch of the Sleeve

thermal resistance, Kapton would have been a material to use for manufacturing the sleeves. However, it would have been challenging to manufacture a seamless sleeve made out of Kapton that wouldn't present any defects.

Instead of using Kapton tubing, the team opted for Uline tubing that matched the exact dimensions needed to wrap the tape springs. Since the tape spring had a flattened width of 32 mm, the tube used could wrap an object with a 32 mm diameter maximum. To maintain the "shearless" property of the booms, three small pieces of tubing were used to wrap the boom instead of a single long sleeve that would have covered its total length.

To construct the shearless boom, an inner tape

spring and an outer tape spring are first attached to the central hub, as shown in Step 1. Since we need four booms, we need to attach four inner tape springs and four outer tape springs. Then, three small wraps are inserted and shrunk around two tape springs using a heat gun to form a boom and achieve a SHEARLEESS boom structure, as shown in Step 2.



Figure 21: Step 1 of Building Shearless Booms



Figure 22: Step 2 of Building Shearless Booms

3.3 Flasher Sheet

The flasher sheets are made from Mylar sheets, a type of high tensile strength polyester film used for its heat resistance, lightweight and foldable properties. These properties make it perfect for packaging in aerospace.

A very stiff tape was applied to each section that required folding to fold the membrane. This tape provided the necessary stiffness to ensure clean folding.

For the prototype, only the first 2 meters around

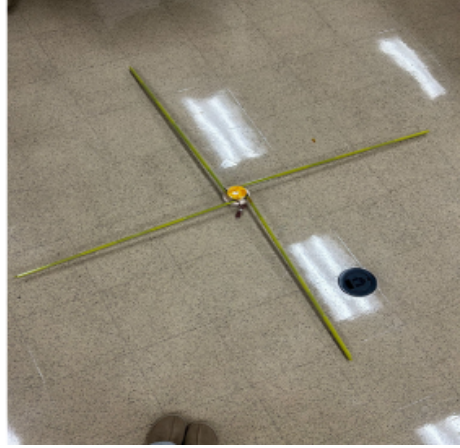


Figure 23: Final Result After Building the Four Booms

the central hub were considered, which reduced the number of mountains and valleys per diagonal to 2 mountains and 1 valley. Figure 24 illustrates the new configuration of the flasher pattern, and Figure 25 shows the flasher pattern built with Mylar sheet when fully deployed.

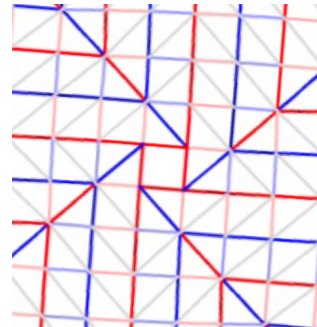


Figure 24: Initial folding creases for the membrane folding. The valleys are blue and the mountains red.

However, the prototype was still too big for testing in the laboratory. Hence, modifications were made to the size of the flasher pattern without impacting any of the work done for the hub. For that, we considered a constant size of the hub on the membrane while reducing the size of the fold cells. The number of fold cells covered by the hub increased from one to four. The new flasher folding reduced the membrane diagonal from 2.80 m to 1.60 m.

Once each membrane was "pre"-creased, the three membranes were folded together (Figure 28) and then attached to each telescoping rod of the booms.



Figure 25: Prototyping and folding of the membrane using Mylar sheet on a smaller scale.

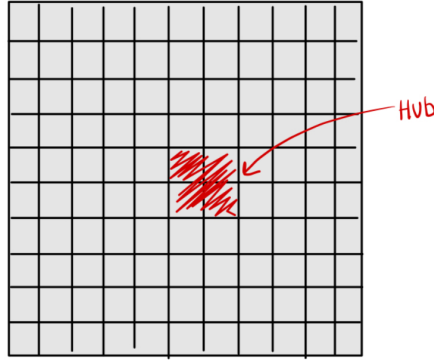


Figure 26: Representation of the number of fold cells covered by the hub



Figure 27: New flasher folding induced by the change in the consideration of the hub.

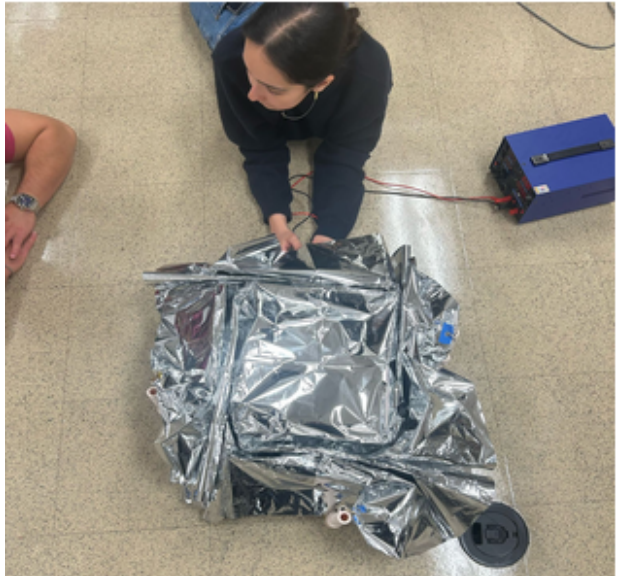


Figure 28: Three membranes folded together

4 Testing

4.1 Boom Testing

The deployment behavior of the prototype bistable booms was evaluated through a series of mechanical tests to assess buckling resistance and coiling/uncoiling performance. Since these booms were constructed using Stanley FATMAX tape measures with three discrete Uline shrink wrap sleeves to approximate the SHEARLESS booms in the flight design, it was necessary to validate their structural integrity and deployment dynamics. Two key tests were conducted: the buckling test, which determined the load at which the boom would fail, and the coiling/uncoiling test, which analyzed how the boom stowed and deployed under controlled conditions.

4.1.1 Buckling Test

To determine the structural limits of the prototype booms, a buckling test was performed by applying incremental loads while the boom was held in a vertical orientation to mimic the tensioning of the membranes. One end of the boom was secured at the base, while the other end was subjected to increasing weights. The applied masses ranged from 128g to 512g, allowing us to pinpoint the threshold at which Euler buckling occurred. Observations showed that at lower applied weights, the boom remained rigid and did not exhibit significant deformation. However, beyond 384g, initial signs of buckling appeared, and by 512g, Euler buckling was observed, and the full structure collapsed. Figure 31 illustrates the observable Euler buckling, and Figure 32 illustrates the full structure collapsed. This established a critical buck-

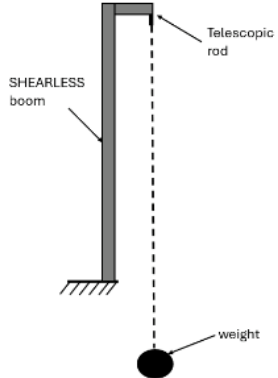


Figure 29: Buckling Test Sketch



Figure 31: Euler Buckling of the Booms



Figure 30: Buckling Test



Figure 32: Full Structure Collapse

ling range between 384g and 512g, providing insight into the structural limitations of the FATMAX tape measure-based booms. Unlike the composite booms in the flight design, which would be optimized for high stiffness with lightweight materials, these prototype booms demonstrated adequate load-bearing capacity for deployment tests but were not designed for high compressive strength.

4.1.2 Coiling/Uncoiling Test

The second phase of testing focused on evaluating the repeatability and control of the coiling and uncoiling process. Since the prototype booms were constructed from Stanley FATMAX steel tape measures, they retained the bistable properties necessary for deployment. However, the integration of the three-section

Uline shrink wrap sleeves required additional validation to ensure smooth extension, retraction, and shearing. To track the deployment motion, Kapton tape markers were placed along the length of the boom. The boom was initially coiled into its stowed configuration, then gradually released to observe its uncoiling motion. The segmented nature of the Uline sleeves was designed to prevent excessive shearing forces while still allowing the boom to extend smoothly. Testing showed that the booms successfully uncoiled without significant irregularities. The FATMAX steel tape provided the necessary bistable properties to drive deployment, while the Uline shrink wrap sleeves allowed controlled extension without excessive resistance. The tape markers confirmed that the motion followed the expected deployment trajectory, and no significant misalignment, twisting, or material failure was observed. The three discrete Uline sleeve sections effectively regulated movement, preventing unwanted bending or unpredictable deployment behaviors.

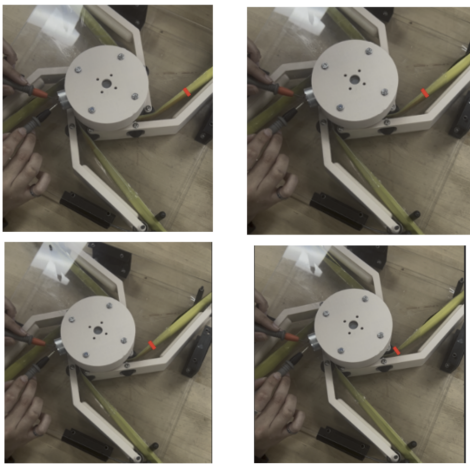


Figure 33: Coiling Tracking

4.1.3 Results

The deployment testing of the prototype booms confirmed that the Stanley FATMAX tape with Uline shrink wrap sleeves effectively approximated the deployment behavior of the flight booms. The buckling test established the structural limitations of the FATMAX-based booms, showing that they could support moderate compressive loads but were not optimized for high-strength applications. The coiling and uncoiling tests demonstrated smooth deployment, with the segmented shrink wrap sleeve design proving effective in preventing excessive shearing while maintaining proper bistable properties. These results validated the feasibility of the prototype boom design for deployment testing, providing critical insights for further refinements and potential improvements to better mimic the flight-ready composite booms.

4.2 Flasher Sheet Deployment Testing

The flasher testing involves unfolding each of the three folded membranes by hand on the floor, which acts as a frictionless support. Figure 34 to Figure 42 illustrate the deployment test of the membrane on the floor.

4.2.1 Results

The results of this test were very positive. We found that the membrane unfolds evenly and totally under low tension. This proved to us that the membrane would unfold with the mechanism in the manner intended.



Figure 34: Membrane deploying test step 1



Figure 35: Membrane deploying test step 2

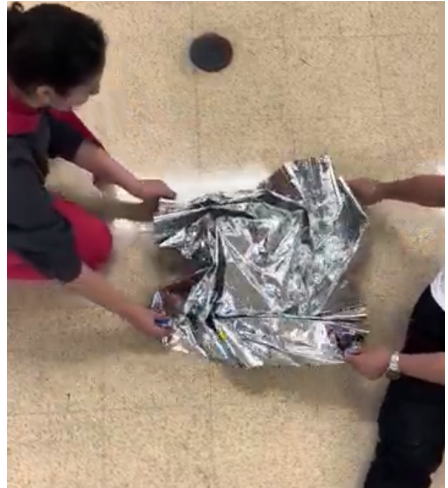


Figure 36: Membrane deploying test step 3



Figure 37: Membrane deploying test step 4



Figure 38: Membrane deploying test step 5



Figure 39: Membrane deploying test step 6



Figure 40: Membrane deploying test step 7



Figure 41: Membrane deploying test step 8



Figure 42: Membrane deploying test step 9

Figure 43: Membrane deploying test.

4.3 Central Hub Testing

The central hub was a critical component in the deployment system, serving as the primary rotational mechanism responsible for uncoiling the booms. Since the hub was directly coupled to the motor, its design and functionality were inherently dependent on the torque, speed, and mechanical connection of the motor to the hub shaft. Any failure in the hub's ability to transmit force effectively would result in deployment issues, making this one of the most rigorously tested components of the prototype. Throughout development, multiple design iterations were tested to optimize the hub's structural integrity, boom integration, and motor compatibility. The primary goals of testing were to ensure that the hub could interface securely with the booms, allow for smooth rotational motion, and withstand the forces required for deployment without mechanical failure. Over the course of development, several significant challenges were encountered, including inadequate motor control, torque transmission failures, and manufacturing defects. Through a systematic process of refinement, these challenges were addressed, leading to a final, functional design that successfully enabled controlled boom deployment.

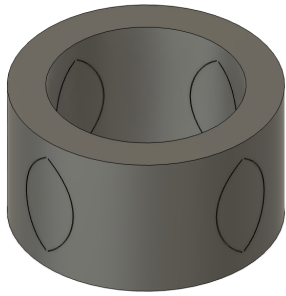


Figure 44: Initial Hub Iteration

4.3.1 Early Hub Geometry and Boom Interface Tests

The first iteration of the hub design was intended to work with a high-RPM brushed DC motor. At this stage, the focus was on ensuring that the booms could be properly fed into the hub and that the motor could generate enough torque to drive the deployment process. The initial design featured slits that allowed the booms to protrude directly outward from the hub, with the assumption that this would provide a secure attachment while allowing for efficient torque transmission. However, initial testing quickly revealed fun-

damental issues with this approach. The protruding booms did not align well with the rotation of the hub, leading to increased resistance and uneven force distribution during deployment. This misalignment created significant mechanical stress, preventing the booms from smoothly uncoiling and causing the system to jam under load. To correct this, the hub was redesigned with a new geometry in which the booms fed into the hub tangentially rather than protruding outward. This adjustment dramatically reduced deployment resistance and improved torque efficiency, allowing the motor to rotate the hub more smoothly. Despite successfully resolving the boom misalignment issue, a more significant problem emerged. The high-RPM motor proved to be unsuitable for controlled deployment, even when used in conjunction with a speed controller. The motor's speed remained too high, resulting in uncontrolled, erratic deployment behavior. The inability to reduce the motor speed sufficiently meant that the entire hub design needed to be modified to accommodate a new motor with a lower rotational speed and higher torque output.

4.3.2 Motor Integration Tests

With the geometry of the hub corrected, attention turned to integrating a lower-RPM geared motor that would allow for a slower, more controlled deployment sequence. This motor provided better torque characteristics and, on paper, seemed to be the ideal solution. However, after designing and manufacturing a new hub specifically for this motor, a new issue emerged—stripping between the motor and the hub shaft. During testing, the hub repeatedly failed to transfer torque effectively, as the connection between the motor shaft and the hub was not secure enough to handle the required force. The rotational motion caused slippage, preventing the hub from rotating properly and halting the deployment sequence. It was unclear at first whether this failure was due to insufficient structural strength of the hub material (PLA) or a poor mechanical interface between the motor shaft and the hub itself. To address this issue, alternative materials were considered in an attempt to improve mechanical strength and precision in the shaft connection. The next logical step was to explore the feasibility of using a resin-printed hub, which offered higher material density and improved surface finish compared to PLA.

4.3.3 Resin Printed Hub Tests

A new iteration of the hub was printed using resin-based 3D printing technology, which was expected to improve precision, durability, and resistance to stripping. This version of the hub was tested under identi-



Figure 45: Resin Printed Hub With Filled Slits

cal conditions to evaluate whether resin could provide a more robust mechanical interface with the motor. However, new challenges arose during the manufacturing process. While the resin hub was printed with greater precision in some areas, the slits for the boom feed-in did not print correctly. These slits were essential for allowing the booms to integrate properly with the hub, and without them, the hub was rendered unusable for further testing. Since the geometry of the hub was critical for smooth deployment, the inability to print accurate slits meant that the resin hub was ultimately discarded as a viable option. Although the resin material itself had potential, the limitations in manufacturing accuracy and print resolution led the team to return to PLA printing while exploring an alternative solution to address the motor shaft stripping issue.



Figure 46: Testing of PLA Hub With Shaft Coupler

4.3.4 PLA Hub With Shaft Coupler

After eliminating the resin hub as a viable option, a final iteration was developed that retained PLA as the primary hub material while incorporating a shaft coupler to improve torque transfer from the

motor. The addition of a shaft coupler allowed for a more secure and mechanically efficient connection, preventing slippage and stripping while still maintaining the required flexibility to accommodate motor movement. This final design was extensively tested under full deployment conditions and successfully resolved all previous issues. The PLA hub, when paired with the shaft coupler, provided reliable torque transfer, and the new motor allowed for slow, controlled deployment of the booms. The tangential feed-in slots worked as expected, ensuring proper alignment and smooth uncoiling throughout the deployment sequence. With this configuration, the central hub successfully fulfilled its intended function, demonstrating stable operation and compatibility with the overall deployment system.

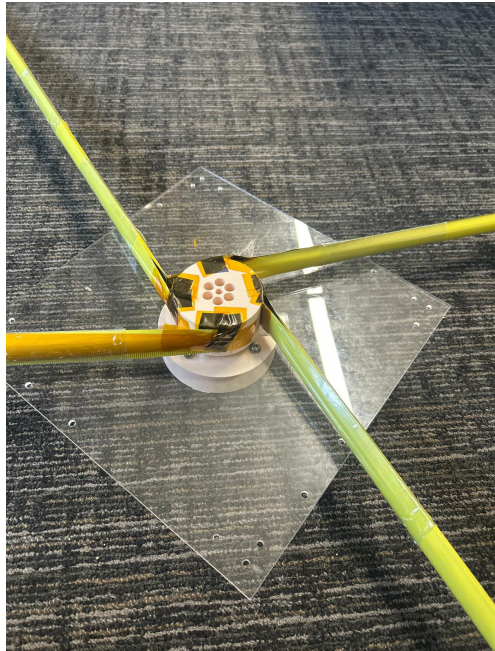


Figure 47: Integration of Final Hub With Booms

4.3.5 Results

Through multiple design iterations and extensive testing, the central hub evolved into a fully functional deployment mechanism that effectively interfaced with both the booms and the motor. The early design failures highlighted critical issues with motor selection, torque transfer, and material properties, which were progressively addressed through geometry refinements, motor upgrades, and structural modifications. The final PLA hub with a shaft coupler emerged as the most reliable solution, eliminating the stripping issues encountered with the earlier motor integration while maintaining a robust and efficient

deployment mechanism. Future improvements could focus on exploring alternative materials to enhance durability and weight reduction, as well as further refining the motor control system to improve precision during deployment.

4.4 Telescoping Rods Testing

The telescoping poles were a crucial structural component in the prototype, responsible for ensuring that the membrane deployed smoothly while maintaining the necessary layer separation. Similar to the flight design, the prototype incorporated telescoping rods to help stabilize the membrane and guide its unfolding process. These rods needed to be lightweight, strong, and capable of extending and retracting smoothly without excessive resistance or instability. Given that the telescoping rods were fabricated using 3D-printed PLA components and spring-loaded mechanisms, extensive testing was required to refine their sliding motion, threaded interfaces, hoop mating features, and spring force behavior. The goal was to iterate through multiple design configurations to identify failure modes and refine the rod performance. Each test focused on a specific aspect of the rod's functionality, with iterative changes made to improve overall performance and integration with the deployment system.

4.4.1 Tolerance Tests

One of the most important design considerations for the telescoping rods was ensuring that the sliding poles could extend and retract without excessive friction or instability. In early prototypes, the inner and outer tubes exhibited inconsistent tolerances, leading to undesirable performance. If the fit was too tight, friction prevented smooth extension, requiring excessive force to deploy. Conversely, if the fit was too loose, the rods lacked stability, allowing for excessive lateral movement that compromised their ability to properly guide the deployment. To refine the tolerances, three iterations of the sliding pole geometry were tested. The first design featured uniform cylindrical tubes, but early tests revealed that minor inconsistencies in the 3D-printed surface finish led to unwanted friction in certain regions of the rod. To address this, the second iteration introduced a slightly increased inner diameter for the outer tube, reducing contact friction while still maintaining a stable guiding structure. The third and final iteration incorporated threaded ends to attach to the boom interface and hoop interface to either ends. After these iterations, the final sliding pole configuration successfully achieved reliable extension and retraction, ensuring that the rods could function effectively within the

deployment system. The tolerances were optimized to prevent excessive friction while maintaining structural stability, leading to a functional design that supported smooth deployment.

4.4.2 Threaded Ends Test

To facilitate easy assembly and secure integration with the surrounding structure, the telescoping rods were designed with threaded ends, as shown in Figure 48. These threads allowed for modular attachment, ensuring that components could be easily replaced or adjusted without requiring an entirely new rod assembly. However, the thread pitch, depth, and engagement mechanism had to be carefully optimized to balance structural strength with ease of assembly.

Two different thread configurations were tested. The initial version featured standard 3D-printed threads, but testing revealed high variability in thread quality due to the limitations of the printing process. The second iteration introduced deeper and wider threads, which improved engagement, refined the thread depth, and included a tapered lead-in, thereby reducing the risk of misalignment during assembly.

The final threaded design (Figure 48) provided a secure connection without excessive friction, ensuring that the rods could be easily installed while maintaining sufficient strength. This optimization improved the overall modularity of the design, allowing for quick component replacement and easier adjustments during assembly and testing.

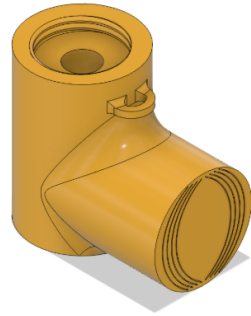


Figure 48: Telescoping End-Boom Interface With Threaded Ends

4.4.3 Hoop Mating Feature

The telescoping rods needed to interface seamlessly with the booms and membrane, requiring a precise hoop mating mechanism. This feature ensured that the rods remained properly connected to the surrounding structure while providing a stable attachment point for the deployment system. The hoop feature needed to accommodate minor misalignments



Figure 49: Top Hoop Mating Attachment

while ensuring a firm connection that prevented unwanted movement during deployment. Therefore, the hoops needed to be placed in precise locations to maintain the 10 cm separation and limit the membrane from shifting. Two variations of the hoop mating design were evaluated, both identical in structure but differing in size. The initial design incorporated an extrusion on three key components: a small threaded end that attached to the smallest telescoping pole, a larger pole featuring an extrusion at its top end, and a third extrusion at the boom-telescope interface, which screwed into the larger pole. The clips used in the prototype were essential for securing the membrane to the telescoping rods while maintaining a stable yet flexible attachment. The selected clips had outer diameters ranging from 1.7 cm (0.67 in) to 2.6 cm (1.02 in), with corresponding inner diameters between 1 cm (0.39 in) and 1.9 cm (0.75 in). These dimensions were chosen to ensure compatibility with the hoop mating features while providing a secure grip on the membrane. Initially, the hoop extrusions were too small to fit the clips properly, leading to an iteration where the extrusions were resized to accommodate the binder clips more effectively. The final configuration ensured a firm yet non-damaging attachment, allowing for reliable membrane support and alignment throughout deployment.

4.4.4 Boom-Pole Interface Test

The interface between the booms and the telescoping poles was a critical design consideration, as it needed to securely hold the deployable booms while allowing for a precise fit that prevented unwanted movement or misalignment. The connection was achieved through slits printed into the end caps of the telescoping rods, which were designed to accommodate the bistable tape-spring booms. Since achieving the correct spacing was crucial for proper alignment and deployment, multiple configurations were tested to determine the optimal interface geometry. To evaluate the best fit, four different spacing options were printed on the ends of the telescoping poles, each with slightly varying slot widths and depths. These variations were intended to balance a secure mechan-



Figure 50: Telescoping End-Boom Interface Testing

ical hold on the booms while avoiding excessive friction or deformation that could impede deployment. The testing process involved manually inserting the booms into each of the four slit configurations and assessing their ability to remain firmly in place while allowing for smooth engagement and disengagement. In the first slit design, the spacing was too narrow, causing difficulty inserting the booms and the booms experienced excessive resistance when being inserted. This created difficulties in assembly and posed the risk of introducing unwanted stress concentrations on the tape springs. The third and fourth configurations, while allowing for easier insertion, did not provide enough grip, leading to undesired lateral play in the connection that could compromise deployment stability. After testing all configurations, the second slit design was determined to be the most effective, as it provided a snug fit without excessive resistance. This version allowed the booms to be inserted smoothly while maintaining a secure hold that prevented shifting or detachment during deployment. The finalized slit spacing was integrated into the telescoping pole design, ensuring that the boom-telescope interface was both structurally sound and functionally reliable for the final prototype.

4.5 Spring Arm Tests

The spring arms played an important role in ensuring a controlled and uniform deployment of the prototype booms. Without sufficient resistance, the booms could extend too rapidly, leading to asymmetric or uncontrolled blossoming, which could introduce stresses, misalignment, or deployment failure. To regulate the motion of the booms, torsion springs were integrated into the spring arms, providing restorative force that resisted excessive movement and maintained deployment stability. A series of tests

were conducted to validate the stiffness of the spring arms, the effectiveness of the torsion springs, and the interaction between the arms, spacers, and rollers.

4.5.1 Spring Stiffness and Deployment Control

The first phase of testing focused on evaluating whether the spring arms could effectively resist excessive boom deployment forces while still allowing for a gradual, controlled extension. Multiple torsion springs were tested to determine the optimal stiffness required to prevent the booms from overextending too quickly. Initially, a softer torsion spring was used, but testing showed that it did not provide sufficient resistance, allowing the booms to expand too rapidly. This uncontrolled expansion compromised the uniformity of deployment, indicating that a stiffer spring was necessary.

4.5.2 Arms, Spacers and Rollers Test

Beyond stiffness, another critical factor in the success of the spring arm system was ensuring proper fit and mechanical integration with the spacers and rollers. The initial iteration of the rollers was found to be too small, resulting in a misalignment that affected the arms' ability to engage smoothly with the deployment mechanism. Through iterative adjustments, the roller dimensions were modified to achieve a better fit, eliminating unnecessary friction while maintaining a firm guiding structure. Several iterations of the spring arms were tested to refine the mechanical engagement between components. Early designs lacked precise alignment between the spacers and torsion springs, leading to uneven force distribution. After three to four iterations, the design was modified to include improved spacer placement and a more secure mounting interface, which ensured that the arms functioned reliably without excessive stress on the torsion springs. These final arms included built in space for the torsional spring to rest inside, ensuring that the outer border of the mechanism would not buckle under the spring energy.

4.5.3 Results

With the stiffer torsion springs and refined roller dimensions, the spring arms successfully regulated the deployment speed and sequence, ensuring that the booms extended evenly and predictably. The final test results confirmed that the system prevented premature blossoming, providing a stable deployment profile that closely mimicked the expected behavior of the full-scale system. The controlled expansion achieved in the final design demonstrated that the spring arms and torsion springs were properly tuned

to maintain a slow, steady deployment, mitigating risks associated with uncontrolled boom extension. Further refinements in spring selection and interface tolerances could improve performance even further, but the current system effectively fulfilled its intended role in stabilizing the deployment process. To ad-



Figure 51: Spring Arm Testing Setup

dress this, a larger and stiffer torsion spring was introduced, significantly improving the resistance provided by the spring arms. With the updated configuration, the booms deployed at a more controlled rate, remaining evenly tensioned throughout the deployment sequence. The increased stiffness of the spring arms ensured that the booms extended in a synchronized manner, preventing any sections from deploying prematurely or inconsistently.

4.6 Spring Test



Figure 52: Spring Used in Design

The packaging component of the telescoping rod design was the internal spring mechanism, which controlled the extension and retraction forces. The spring needed to provide enough force to ensure reliable extension but not so much that it overpowered the surrounding structure or caused instability. Early testing revealed that the initial torsional spring was too strong, leading to overly aggressive extension behavior. Instead of smoothly deploying, the rods ex-

tended too quickly, creating instability that could potentially disrupt the deployment sequence. In one of our initial tests, the spring force caused the topmost hoop mating feature to break as the spring energy was released. The pole with the smaller diameter broke away from the structure as well. The failure of the initial spring highlighted the need for a more controlled deployment mechanism. To address this, we could reduce the spring stiffness in a second iteration, providing a lower but more consistent force that allowed for a smoother extension. We do think that the additional dampening mechanisms might be required to further refine the system. After these tests, it was concluded that the torsional spring force needed further adjustment, and future iterations would focus on fine-tuning the stiffness and potentially integrating a dampening system to achieve the desired deployment behavior. This test was deemed a fail.

4.6.1 Results

Through multiple design iterations, the sliding mechanism, threaded interfaces, and hoop mating features were successfully refined, ensuring that the telescoping rods could extend smoothly and securely. The primary remaining issue was the excessive spring force, which led to unintended rapid deployment. Addressing this issue will require further refinement of the spring stiffness or the introduction of a damping mechanism. Overall, the testing of the telescoping rods provided valuable insights into tolerance optimization, attachment mechanics, and force control. By iterating on sliding fit, thread engagement, and hoop design, the final configuration met the structural and functional requirements necessary for supporting the membrane deployment. Future improvements will focus on further optimizing the spring force and implementing minor refinements to improve long-term durability and performance.

4.7 Gravity Offload Testing

The gravity offload system was implemented to simulate the microgravity environment in which the deployable sunshade would operate. Since full deployment dynamics could not be accurately tested under Earth's gravitational conditions, the offload system was designed to counteract the weight of the structure while allowing for realistic deployment motion. This setup was essential in evaluating deployment reliability, structural stability, and potential failure modes before advancing to further testing stages. The offload system consisted of four linear low-friction rails, each equipped with low-friction carriages, pulleys, and counterweights. These rails allowed the attachment points of the booms to move smoothly while

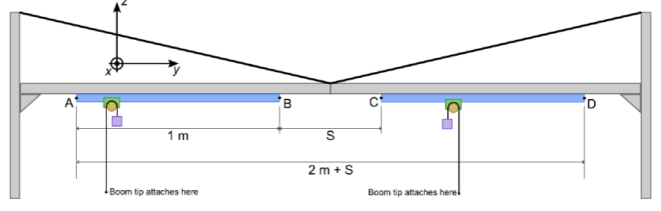


Figure 53: Gravity Offload Sketch for the deployment of the full system

- Linear low-friction rails
- Aluminum rails
- Low-friction carriage
- Pulley
- Counterweight

Figure 54: Legend of the gravity offload sketch for the deployment of the full system

experiencing minimal resistance, effectively mimicking the unconstrained motion expected in a space environment. The boom tips were connected to a counterweighted pulley system, which provided an upward force that balanced the gravitational pull on the structure. The linear rails were each one meter in length, providing a constrained but controlled path for boom motion. The separation distance between the rails, denoted as S , was initially set as a free parameter, allowing for adjustments in the test setup to match the required deployment configuration. Counterweights were carefully selected to offload approximately 25 grams of mass per boom tip, ensuring that the structure experienced a force profile similar to what it would encounter in microgravity. In tuning the separation distance and counterweighting scheme, the system was adjusted to minimize deployment artifacts caused by Earth's gravity while still allowing for clear observation of deployment kinematics and mechanical interactions. The offload system was set up within a controlled indoor environment to minimize external disturbances such as air currents and surface friction. The deployable structure was carefully aligned with the offload rails, and each boom tip was secured to the low-friction carriages. Pulleys and counterweights were then adjusted to provide near-zero net force on the booms, enabling them to extend as if in a weightless environment. To further reduce unwanted mechanical disturbances, the deployment test was conducted on a flat ground surface, ensuring that the sunshade unfolded with minimal external resistance. In addition, to further re-

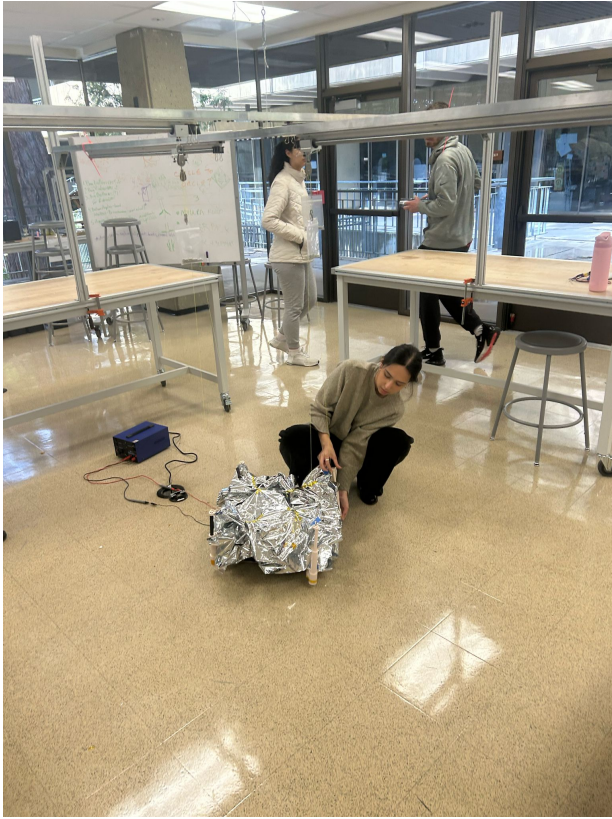


Figure 55: Gravity Offload Setup

duce the deployment angle, deploying from the floor was the best option (also to reduce unwanted tilting). The system was initialized in its stowed configuration, and the deployment sequence was triggered, allowing the booms to extend while being guided by the offload system. During the test, the counterweighting system performed as expected, successfully offloading the gravitational effects and allowing for smooth extension of the booms. The linear rail system provided a stable and repeatable motion path, ensuring that the deployment followed the intended trajectory without significant deviations. However, some minor issues were observed, particularly in the initial extension phase. In certain instances, the booms were caught in the deployment, momentarily forcing the booms beyond their intended trajectory before stabilizing. This effect suggested that further fine-tuning of the counterweight force or damping mechanisms could be beneficial in reducing oscillations. Another factor that influenced deployment behavior was the separation distance between the rails. A larger separation distance resulted in a more uniform unfolding, whereas a smaller separation would lead to slightly constrained movement. Further testing would be required to determine the optimal configuration for

achieving consistent deployment. The gravity offload system successfully simulated a reduced-gravity environment, enabling realistic testing of the deployment mechanics. The low-friction rail and counterweight system effectively minimized external forces, allowing for a clear assessment of the boom extension and membrane unfolding dynamics. The findings from these tests provided critical insights into the real-world behavior of the deployable system, highlighting areas for refinement and validation. Future testing would focus on optimizing counterweight forces and fine-tuning the rail separation to achieve a fully reliable deployment configuration. These insights will be instrumental in refining the final prototype and ensuring that the sunshade performs as expected under actual deployment conditions.



Figure 56: Deployment Results of Gravity Offload Test

5 Conclusions

This report has demonstrated the feasibility and challenges of designing, prototyping, and testing a deployable sunshade suitable for the next generation of space telescopes. By balancing stringent requirements—such as stowed volume, mass limitations, and adequate structural stiffness—our team proposed a three-layer membrane architecture reinforced by four coilable tape-spring booms. The integration of an origami-based flasher pattern and telescoping rods allowed for compact stowage while enabling a controlled, reliable deployment.

Prototyping efforts with scaled-down components, such as Stanley FATMAX tape measures for the booms and Mylar sheets for the membranes, provided insights into design pitfalls and corrective strategies. In particular, multiple iterations of the central hub and motor interface highlighted the importance of

adequate torque transmission and robust geometric alignment, while tests of spring arms, telescoping rods, and tensioning systems helped refine each subsystem. The gravity offload tests further validated that the deployment could proceed with minimal binding when compensating for Earth’s gravity.

Overall, these activities confirm that an origami-inspired approach, combined with bistable composite or tape-spring booms, is a viable solution to packaging and deploying large membranes in space. Nevertheless, several refinements remain to transition this concept to a flight-qualified system. Future work should focus on reducing the weight of key structural elements, integrating improved damping or tension control to minimize dynamic oscillations, and selecting more space-hardened materials (e.g., composite laminates, Kapton, or FEP-based sleeves). With targeted improvements and further ground testing under realistic environmental simulations, this deployable sunshade concept stands poised to meet the stringent demands of future space telescope missions.

References

- [Fer17] Juan M Fernandez. Advanced deployable shell-based composite booms for small satellite structural applications including solar sails. In *International Symposium on Solar Sailing 2017*, number NF1676L-25486, 2017.
- [FSP⁺13] JM Fernandez, Mark Schenk, G Prassinos, VJ Lappas, and SO Erb. Deployment mechanisms of a gossamer satellite deorbiter. In *15th European space mechanisms and tribology symposium, Noordwijk, The Netherlands*, volume 2, pages 3–2, 2013.
- [Lan97] Robert J. Lang. Origami in action. In *Mechanisms Robotics*, number St. Martin’s Griffin, New York, 1997.
- [LMH16] Robert J. Lang, Spencer Magleby, and Larry L. Howell. Single degree-of-freedom rigidly foldable cut origami flashers. *ASME Journal of Mechanisms and Robotics*, 8(3):031005, June 2016.
- [Sta25] Stanley Tools. Stanley FATMAX 25’ Tape Measure Datasheet, 2025. Accessed: March 20, 2025.
- [ZLT⁺13] Shannon A. Zirbel, Robert J. Lang, Matthew W. Thomson, Daniel A. Sigel, Peter E. Walkemeyer, Brian P. Trease, Spencer P. Magleby, and Larry L. Howell. Accommodating thickness in origami-based deployable arrays. *ASME Journal of Mechanical Design*, 135(11):111005, 2013.